Low-field semiclassical carrier transport in semiconducting carbon nanotubes

G. Pennington* and N. Goldsman†
Department of Electrical Engineering, University of Maryland, College Park, Maryland 20742, U.S.A.
(Received 19 November 2004; revised manuscript received 11 March 2005; published 27 May 2005)

The theory of semiclassical carrier transport in semiconducting single-walled carbon nanotubes is presented. The focus is on transport in response to a small, axially applied field. Carriers are considered to scatter with longitudinal, torsional, and radial breathing acoustic phonons. Theory predicts large mobilities and large mean free paths, each increasing with increasing tube diameter. This results from a small effective mass, which varies inversely with the nanotube diameter. In large diameter tubes, the carrier mobility at 300 K is approximately 10^5 cm^2 V s, while the mean free path approaches 0.5−0.8 μm. Results depend on the lattice temperature, Poisson's ratio, and the chirality angle of the nanotube. Theoretical results compare very well with experiments on long semiconducting carbon nanotubes. This indicates that transport in long single-walled carbon nanotubes is likely limited by phonon scattering at temperatures above ≈200 K.

DOI: 10.1103/PhysRevB.71.205318 PACS number(s): 73.63.Fg, 72.20.Fr, 72.20.Dp, 72.10.Di

I. INTRODUCTION

Since carbon nanotubes were discovered in 1991,[1] many transport studies have focused on carrier transport in metallic tubes.[2] Currently, there is immense interest in possible electronic applications for semiconducting carbon nanotubes.[2,3] This has been prompted primarily by the discovery that these materials can be effectively used as active elements in field-effect transistors (FETs).[4] Such devices are particularly advantageous since the nanotube can be isolated from the gate, allowing for a reduction of surface states when compared to conventional FETs. Promising applications for nanotube FETs are in small and fast electronic devices,[5–7] high mobility implants in conventional Si-based FETs,[8] chemical and biological sensors,[9–11] and electron memory elements.[12,13] The performance of these devices, determined by either the switching speed or sensitivity, is expected to improve as the carrier mobility increases.[3,14] Recent experiments have shown encouraging results, indicating that the mobility is exceptionally large in very long semiconducting single-walled carbon nanotubes (SWCNTs).[14] Here, an intrinsic mobility well above 10^5 cm^2 V s was measured for a 325 μm length semiconducting SWCNT at room temperature. In another recent study, a large mobility of 4×10^4 cm^2 V s was measured in a 3 μm length semiconducting carbon nanotube.[15] These high mobility measurements were performed using nanotubes fabricated by chemical vapor deposition, a process which has greatly reduced the defect levels of the material.[2,3]

At the present time many questions still exist regarding the transport properties of mobile charges in semiconducting carbon nanotubes. Ballistic transport has been observed in short, 300 nm tubes.[15] Longer tubes typically show a linear voltage drop along the length of the tube consistent with nonballistic transport.[2,3,12,16] Furthermore, atomic force microscopy measurements show conduction barriers at intervals of ≈100−400 nm along the length of semiconducting tubes.[3,12,16] These barriers are believed to result from the adsorption of charges onto the nanotube surface, and become less prominent as the carrier density increases.[2] It is likely that carrier localization in such barriers would occur at sufficiently low temperatures in semiconducting nanotubes with lengths in excess of 100 nm.

The mean free path (L_m) is the average distance carriers travel before their momentum is randomized by scattering. This length scale is an important indicator of the transport properties of a nanotube. Electrostatic force microscopy measurements on a 5 μm length, 2 nm diameter semiconducting nanotube have predicted a long mean free path of ≈0.7 μm.[3] In comparison, the mean free path in metallic carbon nanotubes has been observed to be even larger,[2,17–19] and ballistic transport has been observed.[2] A larger L_m in metal nanotubes may result from the lack of sensitivity to adsorbed chargers[16] or a reduction in backscattering.[20] If the tube length (L) does not exceed L_m, ballistic transport is possible in semiconducting carbon nanotubes. In the nonballistic regime, transport will be diffusive if L_m does not greatly exceed the carrier phase relaxation length, L_ϕ.[21] Otherwise, if $L \gg L_m \gg L_\phi$, semiclassical transport may occur in a the nanotube. Experiments indicate that the phase relaxation length in multiwalled semiconducting carbon nanotubes is less than 60 nm at room temperature and above.[22,23] Measurements of L_ϕ in single-walled semiconducting carbon nanotubes are currently lacking. Recent experiments[24] do, however, predict strong electron-electron scattering in semiconducting SWCNTs, indicating a short phase relaxation length.

The focus of this work is a study of the transport properties of semiconducting SWCNTs subject to a low applied electric field along the tube axis. This is important in light of possible FET applications for semiconducting nanotubes. Theoretical results are developed for the semiclassical transport[25,26] of carriers subject to scattering with acoustic phonons. Knowledge of this transport regime can facilitate the identification of semiclassical transport properties in nanotube experiments. These conditions may occur in long tubes or when the carrier-phonon scattering rate is large. The latter condition is more likely at elevated temperatures. Experiments do indeed indicate that phonon scattering is important in carbon nanotubes.[19,27–30] Investigation of the semiclassical limit is also relevant in short tubes and at low

temperatures, where important transport parameters such as the momentum relaxation time τ_m and length L_m can be studied. These time-and length scales can be used to determine the limits of ballistic transport in nanotubes. Furthermore, they may give insight into the properties of diffusive transport and charge localization.

The concentration of this work is on phonon-limited transport. Scattering by defects is not considered. Furthermore, since two-body electron-electron scattering does not alter the carrier ensemble in 1D, momentum is relaxed via phonon scattering only. Effects of electron scattering on the carrier system are however assumed. Electron-electron interactions are considered to not only randomize the carrier phase, but also drive the carrier-lattice system to conditions near thermodynamic equilibrium. For a treatment of low-field transport, carriers are limited to just one subbranch in the electronic structure. In the phonon-limited regime, the low-field transport properties of semiconducting SWCNTs are developed as a function of tube diameter, lattice temperature, and tube chirality. Although single-walled tube are not expected to have a diameter in excess of 10 nm,[21] diameters ranging up to 15 nm are considered here since results may be applicable to transport in the outer shell of a multiwalled tube in the limit of small interwall interaction. Chiralities ranging from zigzag to armchair are considered since semiconducting SWCNTs may be very near the armchair orientation. Transport is also related to properties of the SWCNT band structure, in particular the effective mass and nonparabolicity. Both the mobility and mean free path are found to increase if either the tube diameter increases or the temperature decreases. For tube diameters above 5 nm, the variation with diameter is small. At room temperature, the carrier mobility μ and mean free path L_m are approximately 10^5 cm^2 V s and 500–800 nm, respectively, in these larger diameters tubes. Results do, however, depend on the value taken for Poisson's ratio. Below 5 nm, results predict that the mobility and mean free path both decrease rapidly with decreasing diameter. High values for μ and L_m in semiconducting SWCNTs are found to result primarily from a small effective mass for carriers. This means that carriers will move faster in response to an external field and scatter less frequently. Furthermore, μ and L_m both increase with diameter since the effective mass decreases with tube diameter.

Recent transport measurements in a long semiconducting SWCNT (Ref. 14) provide a unique opportunity for comparison with semiclassical results. Using a carrier-phonon interaction energy determined from calculations on the band structure of strained nanotubes,[31,32] theoretical results are found to compare well with the measured mobility. For a 3.9 nm diameter tube, the experimental mobility at room temperature was found to be $\approx 1.5\times 10^5$ cm^2 V s, agreeing well with the theoretical results of $0.9-1.7\times 10^5$ cm^2 V s for a similar diameter tube. The experimental variation of the mobility with temperature agrees very well with theory, indicating that scattering in long semiconducting SWCNTs is likely dominated by phonons above 200 K. The theoretical result for the mean free path, $\approx$600 nm, also agrees well with previously measured results for semiconducting nanotubes.[3] Good agreement with experimental measurements indicates that transport in long tubes may be semiclassical.

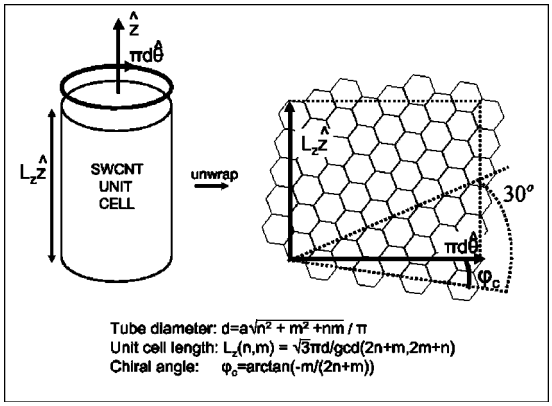

FIG. 1. (Color online) Single-walled carbon nanotube unit cell (Ref. 21). The length and diameter of the unit cell are given in terms of the fundamental tube indices (n,m) and the lattice constant of graphene (a=2.45 Å).

II. LATTICE AND BAND STRUCTURE

For a comprehensive review of the lattice and subband structure of a single-walled carbon nanotube, the reader is directed to Refs. 21 and 33. The unit cell for a single- walled nanotube is illustrated in Fig. 1, where z is along the tube axis and θ is around the tube circumference. The unit cell consists of the cylinder of length L_z, which must be much shorter than the tube length in order to use the semiclassical transport approximations presented in this work. The limits of the chiral angle ϕ_c identify the high-symmetry achiral nanotubes. A minimum angle of 0° occurs in zigzag tubes (m=0), while a maximum angle of 30° is characteristic of armchair tubes ($m=n$). Here (n,m) are the fundamental tube indices. For the remaining achiral tubes, chiral angles range from $0<\phi_c<30°$. The armchair tube is strictly metallic and therefore will not be considered in this work. The largest chiral angle for semiconducting tubes is less than $<30°$ and occurs when $m=n-1$. For convenience, however, ϕ_c will be considered in the full range from 0 to $<30°$ here. In long SWCNTs, physical properties will be independent of the tube length. Furthermore, in some instances, a given physical property will have only a negligible dependence on ϕ_c and may therefore be well approximated as a function of tube diameter alone. This is found to be true for the low-energy band structure relevant for low-field transport in a SWCNT.

The nanoscale diameter of the nanotube leads to carrier confinement around θ, reducing the wave vector space carriers may occupy. This restricted wave vector space is represented as a series of 1D slices as is illustrated in Fig. 2 for the case of a chiral $(n,n)=(4,2)$ tube. Here, the nanotube wave vector space is superimposed onto the hexagonal Brillouin zone of graphene. Each 1D wave vector segment corresponds to a subband in the electronic structure of the nanotube and is characterized by a unique constant value for the circumferential wave vector k_θ. For semiconducting tubes, the wave vector slice nearest to the K point gives the lowest-lying conduction subband for electrons and the highest-lying valence subband for holes. This first subband will be the only subband considered in this work for low-energy, low-field

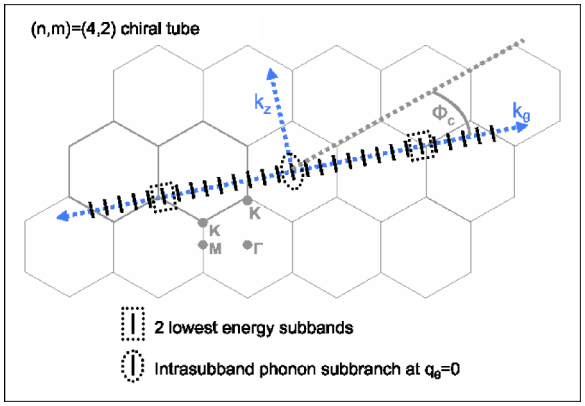

FIG. 2. (Color online) Wave vector space for an $(n,m)=(4,2)$ semiconducting single-walled carbon nanotube (solid line segments), superimposed onto the hexagonal Brillouin zone of graphene.

carrier transport. For any semiconducting tube, as shown in Fig. 2, there are always two degenerate first subbands lying approximately $\pm 2/3$ across the half k-space zone along θ. Limits on the average carrier energy when the one subband model is valid will be discussed at the end of this section.

The wave vector space of a SWCNT near the Fermi point of graphene is shown in Fig. 3. Around the tube circumference, the first subband is separated from the K point by the wave vector Δk_θ. For any semiconducting nanotube, independent of chirality ϕ_c, this separation is given by $\Delta k_\theta = 2/3d$.[33] As the tube diameter increases, Δk_θ decreases and the wave vector space of the SWCNT moves closer to the K point of graphene. The carrier wave vector for the first subband, relative to the Fermi wave vector of graphene $(\vec{k}_F)$, satisfies the following expression:

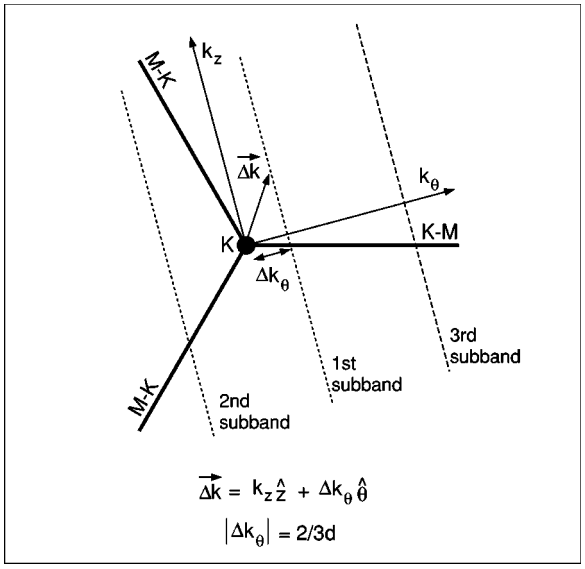

FIG. 3. Wave vector space for a semiconducting single-walled carbon nanotube near the Fermi point of graphene (K) (Ref. 33).

$$\Delta\vec{k} = \vec{k} - \vec{k}_F = k_z\hat{z} + \Delta k_\theta\hat{\theta}, \quad \Delta k_\theta = \frac{2}{3d}. \tag{1}$$

Note that $\Delta\vec{k}$ is dependent on the tube chirality ϕ_c through the directions of the tube axes $\hat{z}$ and $\hat{\theta}$.

The carrier energies of a SWCNT can be accurately determined by zone folding the tight-binding band structure of the graphene π band.[21] The energy (E) in the nanotube can then be found directly from the energy of graphene (E_{2D}) according to the relation $E(\Delta\vec{k}) = E_{2D}(\Delta\vec{k})$.[21] The carrier energy for the first SWCNT subband is therefore determined by E_{2D} near the Fermi point. The graphene energy spectrum here has conical symmetry[33]

$$E_{2D}(k_x,k_y) = (\pm)\beta|\Delta\vec{k}|, \quad |\Delta\vec{k}| < k_{warp}. \tag{2}$$

The above expression for E_{2D} represents the surface of a right circular cone, as shown in Fig. 4(a). The vertex of this cone occurs when both E_{2D} and the wave vector relative to the Fermi point, $\Delta\vec{k}$, are zero. Its slope is given by

$$\beta = \frac{\sqrt{3}\gamma a}{2}, \tag{3}$$

where $a = 2.45$ Å is the lattice constant of graphene. The tight-binding band structure parameter γ is known to be approximately 2.7 eV.[34] The result in Eq. (2) will begin to fail as $\Delta\vec{k}$ moves away from the Fermi point and the band structure cone becomes significantly deformed due to tridiagonal warping. As an upper limit to Eq. (2), the magnitude of the wave vector must be less than k_{warp}. This condition is assumed to be satisfied for low-energy carriers. The range of validity for this approximation is discussed at the end of this section.

Using the zone-folding method, the low-energy subband structure for the carbon nanotube is given by hyperbolic conic sections through E_{2D}. For the first two subbands, this is shown in Figs. 4(a) and 4(b). The conic section for the first subband is described by the expression

$$\left(\frac{2E}{E_{gap}} + 1\right)^2 - \left(\frac{k_z}{\Delta k_\theta}\right)^2 = 1, \tag{4}$$

where the energy gap of the nanotube[21,34] depends on Δk_θ according to

$$E_{gap}(d) = 2\beta|\Delta k_\theta(d)| \propto \frac{\gamma}{d}. \tag{5}$$

The carrier energy E in Eq. (4) is defined relative to the subband minimum at $E_{gap}/2$ for electrons and $-E_{gap}/2$ for holes. Solving for the relative energy gives

$$E(k_z,d) = \pm\frac{E_{gap}(d)}{2}\left[\sqrt{1 + \left(\frac{k_z}{\Delta k_\theta(d)}\right)^2} - 1\right]. \tag{6}$$

For a fixed diameter d, $E(k_z)$ is independent of tube chirality. The range of allowed subband energy states, however, will depend on chirality even when d is fixed. This is because the range of axial wave vectors, $-\pi/L_z \leq k_z \leq \pi/L_z$, is a complicated function of tube chirality (n,m) as seen in Fig. 1.

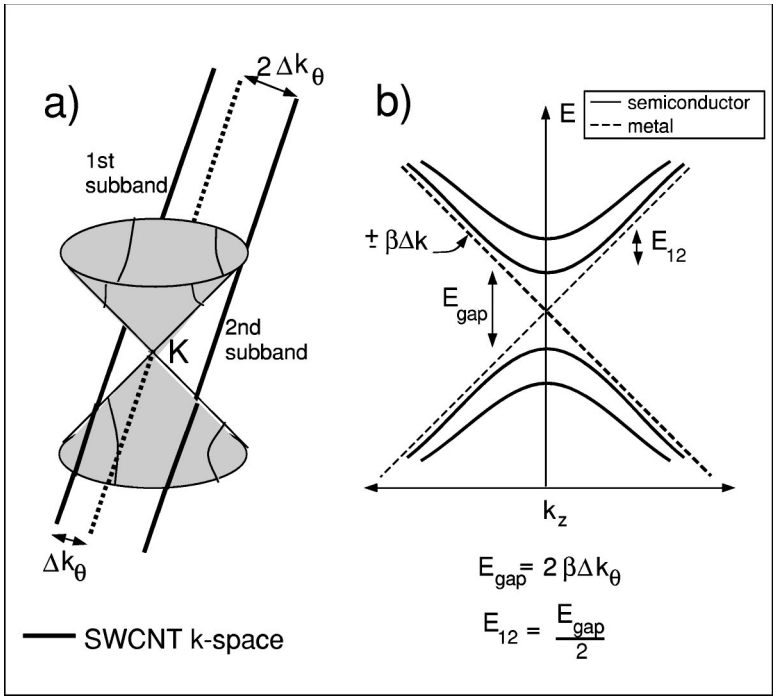

FIG. 4. Band energy for the first and second subbands of a semiconducting single- walled carbon nanotube. Here, Δk_θ is the displacement of k_θ from the K point of graphene, while β is the slope of the low-energy graphene band structure cone.

The low-energy band subband structure of a SWCNT in Eq. (6) agrees exactly with the familiar nonparabolic band shape model

$$\frac{\hbar^2 k_z^2}{m^*(d)} = E(d)[1 + \alpha(d)E(d)], \tag{7}$$

with the corresponding density of states

$$\mathrm{DOS}(E,d) = \frac{\sqrt{m^*}[1 + 2\alpha E]}{2\pi\hbar\sqrt{2E(1 + \alpha E)}}\Theta(E). \tag{8}$$

Here, Θ is a Heaviside step function. By comparing Eq. (6) with the solution for Eq. (7), it can readily be seen that the diameter-dependent nonparabolic factor is equal to the inverse of the band gap

$$\alpha(d) = \frac{1}{E_{gap}(d)}, \tag{9}$$

and thus α is proportional to d/γ. This indicates that the first subband becomes steadily more nonparabolic as the tube diameter increases. When $d \to \infty$, the limit of a graphene sheet, $\alpha \to \infty$ and the band model in Eq. (7) gives $E = \pm\beta|k_z|$. This is the conic section through the vertex of E_{2D} in Eq. (2). The nonparabolic factor determines how close the semiconducting SWCNT is to being metallic. Transport properties presented in this work will be for semiconducting SWCNTs only, where α is finite.

The diameter-dependent effective mass for the first subband in Eq. (7) can also be identified, resulting in the expression

$$m^*(d) = \frac{\hbar^2|\Delta k_\theta(d)|}{\beta} \propto \frac{1}{\gamma d}. \tag{10}$$

It can readily be seen that $m^* \propto 1/\gamma d$ from Eqs. (1) and (5). Note that expressions similar to Eqs. (4) and (5) can be developed for all the subbands if Δk_θ is simply scaled by 1, 2, 4, 5, 7, 8, … . An equation similar to Eq. (7), with a similarly defined m^* and α, can therefore be developed for all the subbands near the Fermi point of graphene. For low-energy transport, however, only the first subband will be used here. The effective mass is an important transport parameter. Since the conduction velocity (v_c) for carriers in the first subband is $\propto 1/m^*(1+2\alpha E)$, the carrier speed should increase with increasing tube diameter when an applied electric field is applied, as long as $E \ll 1/2\alpha$, or equivalently $E \ll E_{gap}/2$. Again, note that E is defined relative to the subband minimum. As E approaches $E_{gap}/2$, the nonparabolic contribution to v_c becomes large and the carrier velocity no longer increases linearly with tube diameter. For comparison among SWCNTs with varying diameters, it is convenient to express m^* in terms of the dimensionless variable $\tilde{d} = d/1$ nm. In terms of $\tilde{d}$, the effective mass of Eq. (10) is

$$m^*(\tilde{d}) = \frac{m_e}{11.37\tilde{\gamma}\tilde{d}}, \tag{11}$$

where m_e is the electronic mass. Allowing for uncertainty in the band structure parameter, the mass here is also given in terms of the dimensionless parameter $\tilde{\gamma} = \gamma/2.7$ eV.

Now, the limits of the band structure model given by Eqs. (7), (9), and (11) will be discussed. This model is valid when only the first subband is significantly occupied with carriers. From conic sections through E_{2D}, the energy spacing between the second and first subbands can be determined as

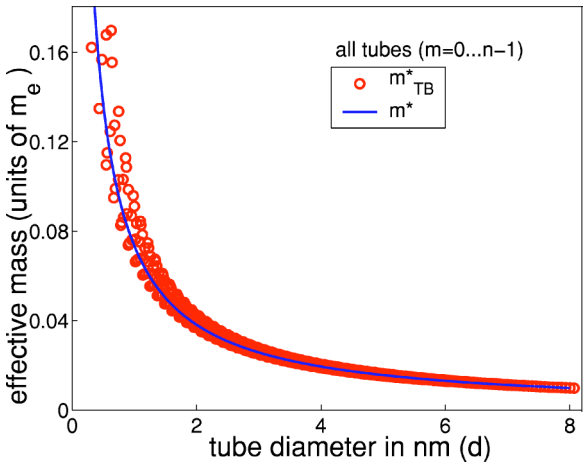

FIG. 5. (Color online) Comparison between the tight-binding effective mass (m^*_{TB}) and the model mass of Eq. (11) (m^*). Semiconducting single-walled carbon nanotubes of all chiralities up to $d=8$ nm are represented.

$$\Delta E_{12} = E_{gap}/2. \tag{12}$$

This is illustrated in Fig. 4(b). The one subband model will therefore be valid when carrier energies E are small compared to $E_{gap}/2$ and for temperatures that satisfy $k_BT \ll \Delta E_{12}$. This condition is less likely to be satisfied as the tube diameter increases and E_{gap} decreases. It is interesting to note that the one subband approximation is valid when the nonparabolic correction to the conduction velocity v_c is small ($E \ll 1/2\alpha$). So, within the framework of the one subband model presented in this work, mobile carriers will move faster as the SWCNT tube diameter increases.

A second limitation on the band model is the validity of Eq. (2) for the low-energy band structure of graphene (E_{2D}). The use of this expression for the first subband of the SWCNT is valid when $|\Delta\vec{k}|$ in Eq. (1) is small compared to k_{warp}. Since Δk_θ and π/L_z both increase as d decreases, tridiagonal warping effects will be more significant in smaller diameter tubes. This can be seen by comparing the model effective mass in Eq. (11) with the result taken from the tight-binding band structure of a SWCNT (E_{TB}).[21] The tight-binding mass can be defined as

$$m^*_{TB} = \hbar^2 \left[\frac{\partial^2 E_{TB}(k_z,k_\theta)}{\partial^2 k_z} \right]^{-1}_{(k_z,k_\theta)=\vec{k}_F+\Delta k_\theta \hat{\theta}}. \tag{13}$$

A comparison in Fig. 5 shows good agreement at large diameters with $d \geq 1$ nm. Below this range, tridiagonal warping begins to become important and m^*_{TB} begins to deviate from the model mass m^*. The effects of warping in the very small diameter tubes will not be considered in this work.

III. DISTRIBUTION AND DENSITY OF MOBILE CARRIERS

The carrier distribution function (f) and the corresponding number density for mobile carriers (N) for the first subband can be developed using the energy model in Eq. (7). The carrier distribution will therefore depend on the tube diameter but not on the tube chirality. When carrier energies are small, near equilibrium, it is reasonable to assume a drifted Maxwellian carrier distribution function

$$f(E) = \exp\left(\frac{-[\sqrt{1+2\alpha|\hbar k_z - \overline{p_z}|^2/m^*} - 1 - \alpha E_F]}{2\alpha k_B T} \right). \tag{14}$$

The Fermi level E_F is set at the Fermi point of graphene if the nanotube is undoped. With energies defined relative to the subband minimum, this gives $|E_F| = E_{gap}/2$. The Maxwellian distribution function in Eq. (14) is valid for an undoped tube when $E_{gap}/2 \gg k_BT$. As mentioned in the previous section, this is indeed true in the one subband limit. Near equilibrium, the average momentum along the tube axis is small and can be expressed in terms of the drift velocity v (Ref. 35)

$$\overline{p_z} = \pm m^* v(1 + \alpha m^* v^2), \tag{15}$$

where the sign is chosen in the direction of the field for holes and opposite the field for electrons. Note that variables for the momentum p_z and wave vector k_z represent both the magnitude and sign of the 1D vector in this work.

It is convenient to express the distribution function in terms of a part symmetric in the momentum and a part asymmetric in the momentum according to $f(E) = f_S(E) + f_A(E)$.[36] To lowest order in $\overline{p_z}$ and to second order in αE, Eq. (14) gives

$$f_S(E) = \exp\left(-\frac{(E - E_F)}{k_B T} \right), \tag{16}$$

and

$$f_A(E) = f_S(E) \frac{\overline{p_z}\hbar k_z}{m^* k_B T} [1 - 2\alpha E(1+\alpha E) + 3(\alpha E)^2]. \tag{17}$$

The expansion for f_A in α can be truncated as shown since the one subband model requires that E be much less than $1/2\alpha$. The density of free mobile carriers (either electrons or holes) when only the first subband is occupied can be readily determined. To second order in $\chi = \alpha k_B T = k_B T / E_{gap}$, the ratio of the thermal to band gap energy

$$N(d,T) = \int_0^\infty \mathrm{DOS}(E) f_S(E) dE = \frac{\sqrt{m^* k_B T/2\pi}}{2\hbar} \left[1 + \frac{3}{4}\chi - \frac{21}{32}\chi^2 \right] e^{-|E_F|/k_B T}. \tag{18}$$

Once averaging over the carrier ensemble, χ will generally be found to give a measure of the significance of nonparabolic band structure effects on the transport properties of a SWCNT. These effects can only be ignored when χ is significantly less than 1. This is more likely for small temperatures and, as mentioned previously, for small tube diameters. Transport properties will be considered up to second order in χ in this work. With dimensionless variables, including

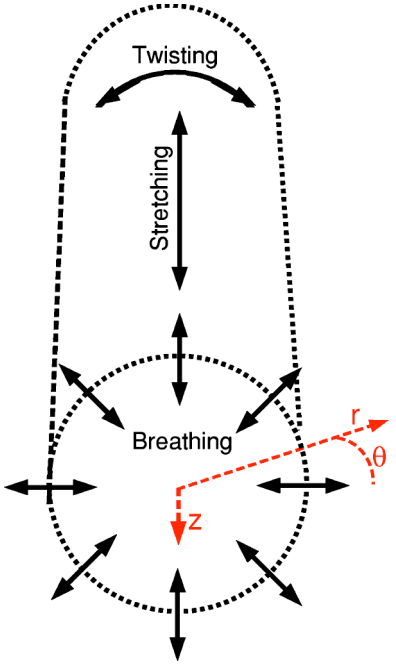

FIG. 6. (Color online) Orientations of long-wavelength acoustic phonon vibrations in a single-walled carbon nanotube.

$\tilde{T}=T/300$ K, the carrier density for undoped nanotube is given by

$$N(\tilde{d},\tilde{T}) = N_0\sqrt{\frac{\tilde{T}}{\tilde{\gamma}\tilde{d}}}\left[1+\frac{3}{4}\chi-\frac{21}{32}\chi^2\right]e^{-1/2\chi}, \quad \chi(\tilde{d},\tilde{T}) \simeq \frac{\tilde{T}\tilde{d}}{30\tilde{\gamma}}. \tag{19}$$

The density parameter is $N_0=3.44\times10^5$ cm^{-1}. Due to the exponential factor, the carrier density is typically very low for an undoped tube even at room temperature. If the nanotube is doped, the exponential factor is reduced and no longer depends on χ. For heavily doping, the carrier density approaches N_0 for a 1 nm diameter tube in the parabolic limit ($\alpha=0$). In this limit, the carrier density is proportional to $1/\sqrt{d}$, decreasing with increasing tube diameter. The parabolic case occurs only when χ is small. When $\tilde{T}=\tilde{\gamma}=1$, the χ series in Eq. (19) is a reasonable approximation for even the largest diameter SWCNTs.

IV. CARRIER-PHONON SCATTERING

As mentioned, experiments indicate that phonons should be a significant source of carrier scattering in metallic carbon nanotubes.[19,27–30] This should also be true in semiconducting tubes. When the carrier energy is low, carriers will scatter predominantly with low-energy, long-wavelength acoustic phonon modes. For a SWCNT these include three important modes, a stretching(L), a twisting(T), and a breathing(B) mode.[21,37] An illustration of these lattice vibrations is given in Fig. 6. The stretching mode mediates deformations of the nanotube along the tube axis in the z direction. It is longitudinally polarized and corresponds closely to the longitudinal acoustic mode in graphene. The twisting mode deforms the nanotube purely along its circumference in the θ direction, and corresponds closely to the in-plane tangential acoustic mode of graphene. This mode is polarized along the tube circumference. Twisting vibrations do not alter the diameter or the length of the tube. For long wavelengths, the phonon energy for both stretching and twisting modes increases linearly with wave vector. These modes therefore have well-defined sound velocities of $v_L=21.1$ km s and $v_T=15$ km s respectively.[21,38] The final acoustic mode considered in this work is the breathing mode. This phonon mode deforms the nanotube radially, altering the effective tube diameter. The breathing mode corresponds to the out-of-plane tangential mode in graphene, but cannot be determined simply by zone folding.[37,39] The results of a continuum model treatment[37] will therefore be used for the acoustic phonon modes. Theory indicates that the particular stretching and breathing phonons relevant for low-field transport are coupled in the long-wavelength limit.[37,38]

The phonon wave vector (q_z,q_θ) is discretized along θ as shown for the carrier wave vector $(\vec{k})$ in in Fig. 2. Whereas each $\vec{k}$ slice corresponds to one distinct carrier subband, each $\vec{q}$ slice corresponds to distinct phonon subbranches, one for each acoustic mode. These subbranches will mediate a specific subband transition of carriers in long tubes where crystal momentum is conserved. Momentum is not only conserved along the tube axis, but also along the tube circumference where carriers and phonons obey periodic boundary conditions. For low-energy, low-field transport, carriers are not able to scatter between degenerate first subbands. There is therefore no change in the k_θ component of the carrier momentum upon scattering with a phonon. Phonons from the wave vector slice in the middle of the zone, crossing the Γ point in Fig. 2, with $q_\theta=0$, will be the relevant phonon subbranches. Since phonon wave vectors are restricted to lie on the 1D segment $\vec{q}=q_z\hat{z}$, the lattice dispacement vector is

$$\vec{u}(z) = (u^L_{q_z}\hat{z} + u^T_{q_z}\hat{\theta} + u^B_{q_z}\hat{r})e^{-iq_z z}. \tag{20}$$

Here, the polarizations of the stretching mode, twisting mode, and coupled breathing vibrations are along $\hat{z}$, $\hat{\theta}$, and $\hat{r}$, respectively.

Since only long-wavelength acoustic phonon scattering is considered, the deformation potential approximation can be used to determine the carrier-phonon scattering rate. Here, the coupling of phonons with the energy structure is considered small and included via the scattering rate. The electron-phonon interaction can be expressed as[37]

$$H_{ep} = -iD_A(S+S^*)/2, \tag{21}$$

with

$$S = \left(\frac{\partial u_z}{\partial z} + i\frac{\partial u_\theta}{\partial z} + \frac{2u_r}{d}\right)e^{3i\phi_c}, \tag{22}$$

and deformation potential D_A. For the $q_\theta=0$ subbranches, a continuum model treatment predicts the coupling of radial and axial displacements in the long-wavelength limit[37]

$$u_{q_z}^B \simeq -i\nu q_z d/2u_{q_z}^L, \tag{23}$$

where ν is Poisson's ratio. Here, a breathing mode vibration accompanies any stretching mode vibration, and vice versa. The relation in Eq. (23) would not be strictly valid if intersubband transitions are considered.[37] The square of the interaction energy in the limit of low phonon energies becomes

$$|H_{ep}|^2 = \frac{D_A^2 k_B T}{2\rho v_L^2 \Omega}\left|(1+\nu)\cos(3\phi_c) - i\frac{v_L}{v_T}\sin(3\phi_c)\right|^2, \tag{24}$$

with unit cell volume $\Omega = \pi L_z d^2/4$. The linear mass density along the tube axis is proportional to the tube diameter according to

$$\rho(d) = 1.89\tilde{d} \times 10^{-14}\text{g cm} = \rho_0\tilde{d}. \tag{25}$$

The results in Eq. (24) are consistent with calculations of the change in the SWCNT band gap with axial and torsional strain[31,32]

$$\left|\frac{d(\text{band gap})}{d(\text{strain})}\right| = 3\gamma(1+\nu)\cos(3\phi_c), \tag{26}$$

and

$$\left|\frac{d(\text{band gap})}{d(\text{shear})}\right| = 3\gamma\sin(3\phi_c). \tag{27}$$

Based on these results, a value of 3γ is used as the deformation potential D_A in Eq. (24). So, the chirality dependence of the carrier-phonon interaction cannot be represented as a simple function of tube diameter. This will therefore also be true for transport properties that depend on the carrier-phonon interaction.

Since the carrier and phonon wave vectors are confined to 1D line segments, carrier-phonon scattering will be restricted due to a reduction in momentum conserving final states. Considering a carrier initially with energy and wave vector (E,k_z) scattering to a final state (E',k_z'), conservation of energy requires

$$\frac{\hbar^2 k_z'^2}{2m^*(1+\alpha E')} = \frac{\hbar^2 k_z^2}{2m^*(1+\alpha E)} (\mp)\hbar v_s|q_z|, \tag{28}$$

using Eq. (7). The sound velocity (v_s) may be either v_L or v_T for L or T scattering, respectively. The upper sign in brackets $(\mp)$ is for phonon absorption, the lower sign for phonon emission. Conservation of crystal momentum in long SWCNTs requires

$$k_z' = k_z + q_z. \tag{29}$$

Solving Eqs. (28) and (29) simultaneously for the final wave vector after scattering gives

$$k_z' = \frac{-k_z(1+2\alpha m^* v_s^2)(\pm)2m^* v_s[1+2\alpha E(k_z)]/\hbar}{1-2\alpha m^* v_s^2}. \tag{30}$$

Since $2\alpha m^* v_s^2 \ll 1$, this is simplified to

$$k_z' \simeq -k_z(\pm)\frac{2m^* v_s}{\hbar}(1+2\alpha E(k_z)) = -k_z(\pm)\Delta k_z. \tag{31}$$

At low fields, carriers are therefore restricted to backscatter within the same subband only. These collisions are essentially elastic when $|\Delta k_z| \ll |k_z|$.

The rate at which carriers scatter at low fields can be developed using Fermi's golden rule.[25] If collisions are approximated as elastic, the backscattering rate is

$$\frac{1}{\tau(E,d)} = \frac{2D_A^2 \pi k_B T}{\hbar\rho(d)v_L^2} F_{\phi_c}\text{DOS}(E,d), \tag{32}$$

which includes both emission and absorption of both L and T phonon polarizations. Strictly the density of states (DOS) blows up at $E=0$, and should be broadened.[25] Since the relevant results of this work are ensemble averages, broadening is not found to be significant and is therefore not included here. The chirality (ϕ_c) dependence is represented by the factor

$$F_{\phi_c} = (1+\nu)^2\cos^2(3\phi_c) + \left(\frac{v_L}{v_T}\right)^2\sin^2(3\phi_c). \tag{33}$$

For the achiral nanotubes, the first term above vanishes in armchair tubes while the second term vanishes in zigzag tubes. Both terms are needed for chiral tubes. The scattering rate increases as ν increases in zigzag and chiral tubes. Theoretically, results for Poisson's ratio vary.[40] Values as small as 0.026 (Ref. 41) and as large as 0.367 (Ref. 42) have been reported. In the former case, the rate in Eq. (32) for armchair tubes would be almost twice as large as that in zigzag tubes. In the latter case, the rate in armchair tubes would only be about 10% larger. Most studies indicate that ν is either close to 0.2,[43–47] the value in graphene, or close to 0.3.[48–51] Since ν is likely less than $(v_L/v_T)-1 \simeq 0.4$, the scattering rate should increase as ϕ_c increases.

V. LOW-FIELD TRANSPORT

Under steady-state, spatially homogeneous conditions, the rate at which carrier momentum is lost via phonon scattering equals the rate at which momentum is gained from an external electric field. As mentioned, electron-electron scattering does not relax the carrier momentum, while defects are not considered in this work. For a SWCNT with an electric field ξ applied along the tube axis, momentum balance is expressed as

$$\hbar\left\langle\left\langle\frac{dk_z}{dt}\right\rangle\right\rangle = -|e|\xi, \tag{34}$$

with the elementary charge of the electron e. The double brackets indicate an average over an ensemble of carriers. At low fields, the rate of momentum loss resulting from collisions with phonons is

$$\frac{dk_z}{dt} = -\frac{[2k_z+\Delta k_z]}{2\tau} - \frac{[2k_z-\Delta k_z]}{2\tau} = -\frac{2k_z}{\tau}, \tag{35}$$

where the change in wave vector is $dk_z = -2k_z(\pm)\Delta k_z$ according to Eq. (31). This includes phonon absorption $(+)$ and

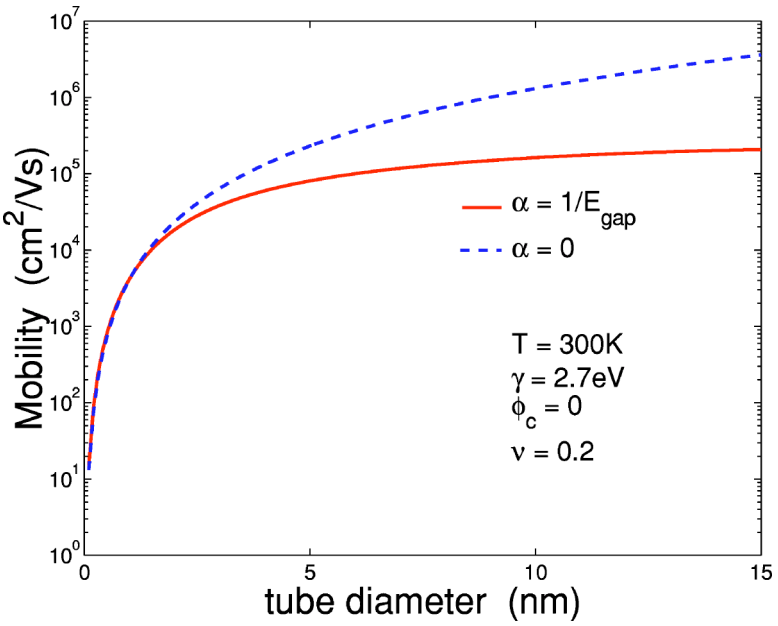

FIG. 7. (Color online) Effects of subband nonparabolicity on the model low- field mobility in Eq. (40). Nonparabolic effects decrease the mobility more significantly as the tube diameter increases. Results are shown at room temperature for a chiral angle and Poisson's ratio of 0° and 0.2, respectively.

emission $(-)$, each with the scattering rate $1/2\tau$ from Eq. (32). The ensemble average is

$$\hbar\left\langle\left\langle\frac{dk_z}{dt}\right\rangle\right\rangle = -\frac{2\hbar}{N}\int_0^\infty \mathrm{DOS}(E) f_A(E)\frac{k_z}{\tau}dE. \tag{36}$$

Note that the contribution due to the Fermi level, $\exp(-E_F/k_BT)$, cancels in the numerator and denominator above. Transport is therefore unaffected by changes in doping when the distribution function in Eqs. (16) and (17) is valid.

Using Eqs. (8), (15), (17), (18), and (32)

$$\hbar\left\langle\left\langle\frac{dk_z}{dt}\right\rangle\right\rangle = \frac{-D_A^2 F_{\phi_c} m^* v(1+\alpha m^* v^2)\sqrt{2m^* k_B T/\pi}}{\rho\hbar^2 v_L^2 F_\chi}. \tag{37}$$

Keeping terms up to second order in $\chi = \alpha k_B T$, the χ factor is

$$F_\chi(d,T) = \frac{1+\frac{3}{4}\chi - \frac{21}{32}\chi^2}{1+2\chi+30\chi^2}. \tag{38}$$

As in Eq. (19), the numerator is a truncated series in χ with terms kept up to second order. Since $\alpha m^* v^2 \ll 1$, Eq. (37) can be solved for the drift velocity, which according to Eq. (34) increases linearly with the electric field. A field-independent low-field mobility can then be defined as

$$\mu = v/\xi = \frac{|e|\rho\hbar^2 v_L^2 F_\chi}{D_A^2 F_{\phi_c} m^* \sqrt{2m^* k_B T/\pi}}, \tag{39}$$

and in terms of dimensionless variables

$$\mu(\tilde{d},\tilde{T},\phi_c) = \mu_0 \frac{\tilde{d}^{5/2}}{\sqrt{\tilde{T}\tilde{\gamma}}}\frac{F_\chi(\tilde{d},\tilde{T})}{F_{\phi_c}}. \tag{40}$$

Here, $\mu_0 = 7.6\times10^3$ cm^2 V s, is the room temperature low-field mobility for a SWCNT with $F_{\phi_c}=1$, $d=1$ nm, $\alpha=0$, and $\gamma=2.7$ eV. The mobility is large in semiconducting SWCNTs since the effective mass m^* in Eq. (11) is rather small. A small mass translates into faster carrier speeds. Scattering rates are also smaller since the density of final states after scattering is proportional to $\sqrt{m^*}$ in Eq. (8). At low fields, when the one electronic subband model is valid, the mobility increases with increasing tube diameter since $\rho/(m^*)^{3/2}$ increases as $d^{5/2}$. The mobility is seen to be the largest in zigzag SWCNTs and the smallest in armchair tubes since $\mu \propto 1/F_{\phi_c}$. This difference is more pronounced if Poisson's ratio is small. As ν approaches 0.4, the mobility becomes essentially independent of chirality ϕ_c. The diameter dependence of μ at room temperature is shown in Fig. 7. The nonparabolic factor α enters Eq. (40) through F_χ. As the diameter increases, this correction increases, and the SWCNT mobility is reduced when compared to the parabolic limit ($\alpha=0$). In tubes with $d>5$ nm, nonparabolic effects are larger and the mobility varies only slowly with diameter approaching $\approx 10^5$ cm^2 V s at 300 K in large tubes ($d>10$ nm). As seen in Fig. 8, the significance of this nonparabolic effect increases with increasing temperature.

It is useful to compare theoretical results for the low-field mobility with experiments. Recently, the temperature-dependent low-field mobility of a 325 μm long, 3.9 nm diameter SWCNT has been measured.[14] Here, the SWCNT was used as the inductive charge channel of a field-effect transistor. The experimental setup is depicted in Fig. 9. With no gate field, the measured mobility for low source-to-drain biasing was found to be very large, approximately 1.5×10^5 cm^2 V s at 300 K. This is about ten times larger than the mobility of graphite.[52]

The chirality or lattice structure of the measured SWCNT was not known, but a diameter of 3.9 nm does correspond closely to an $n=50$ zigzag tube. As can be seen in Fig. 7, theory indicates that the nonparabolicity of the band structure is just beginning to significantly affect the mobility when the tube diameter is 3.9 nm. In Fig. 10, the experimental mobility[14] and the theoretical results of Eq. (40) for a SWCNT are shown together as a function of temperature.

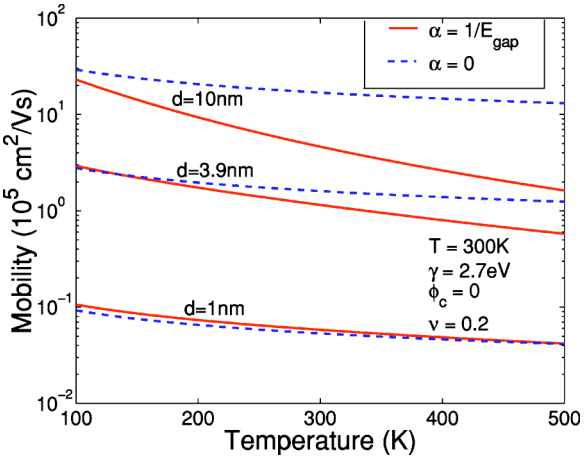

FIG. 8. (Color online) Effects of subband nonparabolicity on the model low- field mobility in Eq. (40). Nonparabolic effects decrease the mobility more significantly as the temperature increases. Results are shown at room temperature for a chiral angle and Poisson's ratio of 0° and 0.2, respectively.

These are the measurements with no gate voltage applied to the SWCNT-FET. The theoretical mobility is given for the extreme chirality cases of $\phi_c = 0°$ and 30°. Results are also given with a Poisson's ratio of 0 and 0.34. The temperature dependence of the theoretical results agrees well with experimental results above 150 K. Experimental results are found to agree best with the phonon scattering results of Eq. (40) when Poisson's ratio is small. At very low temperatures ($\leqslant$150 K), the measured mobility in Fig. 10 does not agree with theory. Phonon scattering appears to no longer be the dominant scattering mechanism. Defect scattering likely limits the mobility at these temperatures. The similarity between the measured and theoretical temperature dependence of μ at low fields is a good indicator that transport may likely be governed by phonon scattering in long SWCNTs at temperatures above 200 K.

Results from the phonon scattering model can be used to obtain the corresponding relaxation time τ_m, defined as the ensemble-averaged time over which carrier momentum is randomized by elastic phonon scattering. The momentum relaxation time can be determined by dividing the average carrier momentum by the rate at which momentum is lost via phonon scattering. In the steady state, where the momentum lost to phonon scattering equals the momentum gained from the applied field, the relaxation time is

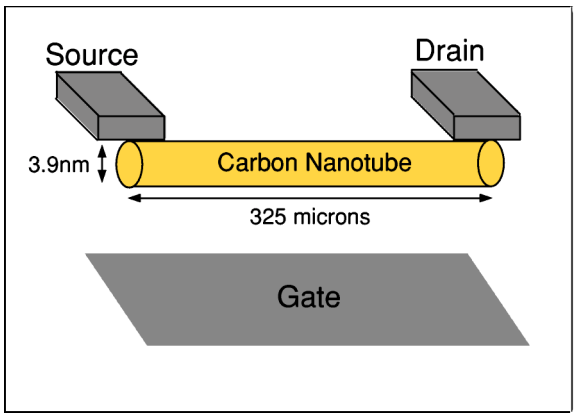

FIG. 9. (Color online) SWCNT-FET of Ref. 14.

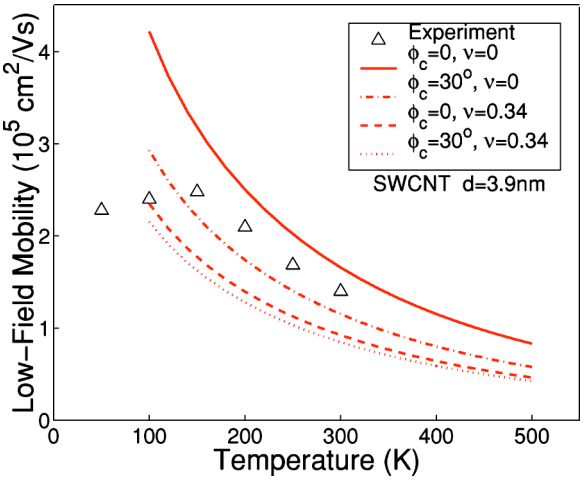

FIG. 10. (Color online) Comparison of the model low-field mobility in Eq. (40) with the experimental results of Ref. 14. Results using maximum and minimum values for the chiral angle ϕ_c and Poisson's ratio ν are given. The theoretical results use a value of 2.7 eV for the hopping integral γ.

$$\tau_m = \frac{\overline{p}}{\hbar\left\langle\left\langle \frac{dk_z}{dt}\right\rangle\right\rangle} = \tau_{m0}\frac{\tilde{d}^{3/2}}{\sqrt{\tilde{T}\tilde{\gamma}}}\frac{F_\chi(\tilde{d},\tilde{T})}{F_{\phi_c}}, \tag{41}$$

with $\tau_{m0} = 3.43 \times 10^{-13}$ s. Since each scattering event is a momentum relaxing backscattering event at low carrier energies, Eq. (41) could also be found by taking the ensemble average of the scattering time τ in Eq. (32). So, as found for the carrier mobility, τ_m is predicted to decrease with increasing chiral angle ϕ_c. Both transport properties are therefore reduced by a factor of $\approx 2/(1+\nu)^2$ on going from a zigzag to an armchair tube. The relaxation time is also predicted to increase with increasing tube diameter. There is, however, a slower increase when compared to μ.

The relaxation time can be used to find the corresponding momentum relaxation length, or meanfree path, L_m. This is the average distance carriers travel before momentum is relaxed by elastic phonon scattering. The mean free path can be found from the thermal velocity (V_{th}) at low fields when the drift velocity can be neglected. It can be expressed as

$$L_m = \langle\langle V_{th}\rangle\rangle \tau_m, \tag{42}$$

where the average random velocity over the ensemble of carriers must be considered since the thermal velocity, $V_{th} = \sqrt{k_B T/m^*(1+2\alpha E)}$, depends on the carrier energy. The ensemble averaged thermal velocity is

$$\langle\langle V_{th}\rangle\rangle = \frac{1}{N}\int_0^\infty \mathrm{DOS}(E) f_S(E) \sqrt{k_B T/m^*(1+2\alpha E)}\, dE$$

$$= \sqrt{k_B T/m^*}\left[\frac{1+\frac{1}{4}\chi-\frac{15}{32}\chi^2}{1+\frac{3}{4}\chi-\frac{21}{32}\chi^2}\right]. \quad (43)$$

The mean free path can be used to define the limits of semiclassical transport in a SWCNT. In this regime, the tube length should be much larger than L_m. Furthermore, the phase relaxation length (L_ϕ), due to carrier-carrier scattering, should be much shorter than L_m. This would indicate a high carrier-carrier scattering rate compared to $1/\tau_m$. As mentioned, recent experiments do indicate strong electron-electron interactions in semiconducting carbon nanotubes.[24] In the semiclassical limit, both carriers and phonons can be represented as wave packets with a well-defined crystal momentum that is conserved in all interactions. Here, results for the transport properties such as the mobility μ in Eq. (40), or the corresponding diffusion constant $D=k_B T\mu/e$, will be valid. The length scales L_m and L_ϕ determine when quantum interference effects enter the transport properties of a SWCNT. If the phase relaxation length exceeds L_m in long nanotubes, transport will be diffusive and carriers will be localized along the tube.[21,2] Here, the carrier-carrier or carrier-defect scattering rate would be less than the phonon scattering rate. The mean free path L_m also gives the limits of ballistic transport in short SWCNTs, where the tube length does not exceed L_m or L_ϕ. In this regime carriers transverse the SWCNT without scattering.

To determine the mean free path for elastic phonon scattering at low fields, the thermal velocity in Eq. (43) is substituted into Eq. (42). Using Eq. (41), this gives

$$L_m \simeq 81.7\ \mathrm{nm} \times \frac{\tilde{d}^2}{\sqrt{\tilde{\gamma}} F_{\phi_c}}\left[\frac{1+\frac{1}{4}\chi-\frac{15}{32}\chi^2}{1+2\chi+30\chi^2}\right]. \quad (44)$$

As found for other semiclassical transport properties, μ and τ_m, the mean free path increases with increasing tube diameter. Again, this occurs since the effective mass is inversely proportional to the tube diameter. Furthermore, a long mean free path results from the small effective mass of a semiconducting SWCNT. As for the mobility and relaxation time, L_m also decreases with increasing chiral angle ϕ_c and increasing ν. In Figs. 11 and 12, L_m is plotted as a function of tube diameter and temperature. There is an increase with increasing d, but the mean free path is eventually found to approximately level off with increasing diameter. At room temperature, d increases to 0.5–0.8 μm, depending on ν. This compares well with experimental results in semiconducting carbon nanotubes where L_m was found to be $\simeq$0.7 μm.[2] In metals, a low-field mean free path of 1.6 μm has been measured.[19] From Eq. (44), L_m is independent of temperature if the nonparabolic band structure factor α is neglected. In the larger tubes, α reduces the mean free path significantly as seen in Fig. 12, where 0.2 is used for Poisson's ratio. For the experimental tube with $d=3.9$ nm, L_m drops approximately linearly from $\approx$0.9 μm to $\approx$0.4 μm as the temperature increases from 100 to 500 K. Since these distances are much less than the tube length, 325 μm, results are consistent with the semiclassical theory presented in this work.

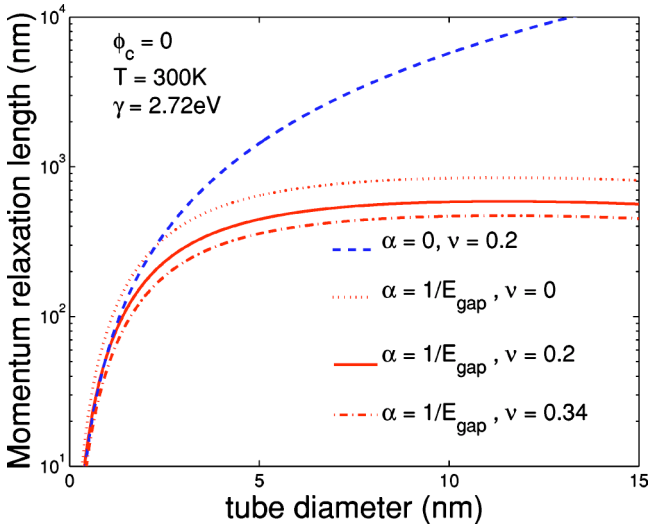

FIG. 11. (Color online) Effects of subband nonparabolicity on the model low-field momentum relaxation length (L_m) in Eq. (44). Nonparabolic effects decrease L_m more significantly as the tube diameter increases. Results are shown for a range of values for Poisson's ration ν. The lattice temperature and chiral angle are fixed at 300 K and 0°, respectively.

VI. CONCLUSION

In light of applications in nanoelectronic devices, an understanding of carrier transport in semiconducting carbon nanotubes is important. In this work we have presented the semiclassical theory for carrier transport at low fields in

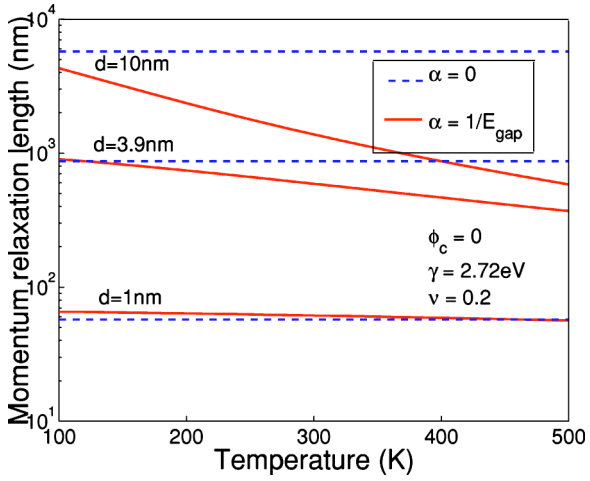

FIG. 12. (Color online) Effects of subband nonparabolicity on the model low- field momentum relaxation length (L_m) in Eq. (44). Nonparabolic effects decrease L_m more significantly as the temperature increases. Results are shown at room temperature for a chiral angle and Poisson's ratio of 0° and 0.2, respectively.

semiconducting SWCNTs. Treatment has focused on the phonon-limited transport regime where carrier scattering is dominated by long-wavelength acoustic phonons. Here, carriers scatter with longitudinal, torsional, and radial breathing phonon modes. Transport properties are related to the carrier-phonon interaction and to the band structure properties of the nanotube. Large mobilities and large mean free paths result from the small effective mass characteristic of semiconducting SWCNTs. Since m^* varies inversely with tube diameter, both μ and L_m are found to increase with increasing tube diameter. The nonparabolicity of the band structure, however, increases as the tube diameter increases, leading to near saturation of μ and L_m with increasing diameter. For large diameter tubes (>10 nm), these transport properties approach 10^5 cm^2 V s and 0.5–0.8 μm, respectively. These result agree very well with experimental measurements.[3] The mobility in long semiconducting SWCNTs appears to be well above typical values observed in conventional Si devices ($\approx 10^3$ cm^2 V s).[3]

Furthermore, the carrier mobility and mean free path both decrease with increasing lattice temperature. The effect is more pronounced in larger diameter tubes where nonparabolic effects play a larger role. In fact, L_m is found to be independent of temperature in the purely parabolic limit. A chirality dependence enters the semiclassical transport properties of semiconducting SWCNTs through the carrier-phonon interaction. The band structure is approximately independent of chirality in the low-field approximation. Transport is found to be more strongly dependent on chirality for small values of Poisson's ratio. The mobility and mean free path both decrease with increasing chiral angle, and are therefore smallest in armchair tubes and largest in zigzag tubes.

The effects of doping are not considered in this work. Reported transport properties should, however, only alter in the case of heavy doping. This would occur when the Fermi level reaches the energy of the subband minimum. When the distribution of carriers is well described using a drifted Maxwellian, transport is independent of doping levels. As mentioned, theoretical results are found to compare very well with experiments on long semiconducting carbon nanotubes. Comparison indicates that transport in long single-walled carbon nanotubes is likely limited by phonon scattering at temperatures above ≈ 200 K. Good agreement with experimental measurements also suggests that transport in long semiconducting single-walled carbon nanotubes may be described using semiclassical approximations.

ACKNOWLEDGMENT

The authors thank M.S. Fuhrer for useful discussions pertaining to this work.

*Email address: garyp@glue.umd.edu
†Email address: neil@eng.umd.edu

[1] S. Iijima, Nature (London) **354**, 56 (1991).
[2] P. L. McEuen, M. S. Fuhrer, and H. Park, IEEE Trans. Nanotech. **1**, 78 (2002).
[3] T. Durkop, B. M. Kim, and M. S. Fuhrer, J. Phys.: Condens. Matter **16**, R553 (2004).
[4] S. J. Tans, A. R. M. Verschueuren, and C. Dekker, Nature (London) **393**, 49 (1998).
[5] A. Bachtold, P. Hadley, T. Nakanishi, and C. Dekker, Science **294**, 1317 (2001).
[6] P. Avouris, J. Appenzeller, R. Martel, and S. J. Wind, Proc. IEEE **91**, 1772 (2003).
[7] J. Appenzeller, J. Knoch, R. Martel, V. Derycke, S. J. Wind, and P. Avouris, IEEE Trans. Nanotech. **1**, 184 (2002).
[8] A. Akturk, G. Pennington, and N. Goldsman, Third IEEE Conf. on Nanotech., 24 (2003).
[9] P. G. Collins, K. Bradley, M. Ishigami, and A. Zettl, Science **287**, 1801 (2000).
[10] J. Kong, N. R. Franklin, C. Zhou, M. G. Chapline, S. Peng, K. Cho, and H. Dai, Science **287**, 622 (2000).
[11] A. Star, J. P. Gabriel, K. Bradley, and G. Gruner, Nano Lett. **3**, 459 (2003).
[12] M. S. Fuhrer, B. M. Kim, T. Durkop, and T. Brintlinger, Nano Lett. **2**, 755 (2002).
[13] M. Radosavljevic, M. Freitag, K. V. Thadani, and A. T. Johnson, Nano Lett. **2**, 761 (2002).
[14] T. Durkop, S. A. Getty, E. Cobas, and M. S. Fuhrer, Nano Lett. **4**, 35 (2004).
[15] A. Javey, J. Guo, Q. Wang, and M. Lundstrom, Nature (London) **424**, 654 (2003).
[16] P. L. McEuen, M. Bockrath, D. H. Cobden, Y. G. Yoon, and S. G. Louie, Phys. Rev. Lett. **83**, 5098 (1999).
[17] S. J. Tans, M. H. Devoret, H. Dai, A. Thess, R. E. Smalley, L. J. Geerligs, and C. Dekker, Nature (London) **386**, 474 (1997).
[18] J. Kong, C. Zhou, A. Morpurgo, H. T. Soh, C. F. Quate, C. Marcus, and H. Dai, Appl. Phys. A: Mater. Sci. Process. **69**, 305 (1999).
[19] J. Y. Park, S. Rosenblatt, Y. Yaish, V. Sazononva, H. Ustunel, S. Braig, T. A. Arias, P. W. Brouwer, and P. L. McEuen, Nano Lett. **4**, 517 (2004).
[20] T. Ando and H. Suzuura, Physica E (Amsterdam) **18**, 202 (2003).
[21] R. Saito, M. S. Dresselhaus, and G. Dresselhaus, *Physical Properties of Carbon Nanotubes* (Imperial College Press, London, 1998).
[22] C. Schonenberger, A. Bachtold, C. Strunk, J. P. Salvetat, and L. Forro, Appl. Phys. A: Mater. Sci. Process. **69**, 283 (1999).
[23] B. Stojetz, C. Hagen, C. Hendlmeier, E. Ljubovic, L. Forro, and C. Strunk, New J. Phys. **6**, 27 (2004).
[24] P. Jarillo-Herrero, S. Sapmaz, C. Dekker, L. P. Kouwenhoven, and H. S. J. van der Zant, Nature (London) **429**, 389 (2004).
[25] G. Pennington and N. Goldsman, Phys. Rev. B **68**, 45 426 (2003).
[26] G. Pennington and N. Goldsman, IEICE Trans. Electron. **E86-C**, 372 (2003).
[27] T. Hertel and G. Moos, Phys. Rev. Lett. **84**, 5002 (2000).
[28] Z. Yao, C. L. Kane, and C. Dekker, Phys. Rev. Lett. **84**, 2941 (2000).

[29] J. Appenzeller, R. Martel, and P. Avouris, Appl. Phys. Lett. **78**, 3313 (2001).
[30] C. L. Kane, E. J. Mele, R. S. Lee, J. E. Fischer, P. Petit, H. Dai, A. Thess, R. E. Smalley, A. R. M. Verschueren, S. J. Tans, and C. Dekker, Europhys. Lett. **41**, 683 (1998).
[31] L. Yang, M. P. Anantram, J. Han, and J. P. Lu, Phys. Rev. B **60**, 13874 (1999).
[32] L. Yang and J. Han, Phys. Rev. Lett. **85**, 154 (2000).
[33] J. W. Mintmire and C. T. White, Phys. Rev. Lett. **81**, 2506 (1998).
[34] C. T. White and J. W. Mintmire, Nature (London) **394**, 29 (1998).
[35] R. C. Curby and D. K. Ferry, Phys. Rev. B **3**, 3379 (1971).
[36] M. Lundstrom, *Fundamentals of Carrier Transport* (Addison-Wesley, Reading, MA, 1990).
[37] H. Suzuura and T. Ando, Phys. Rev. B **65**, 235412 (2002).
[38] T. Ando, Int. J. High Speed Electron. Syst. **13**, 849 (2003).
[39] R. A. Jishi, L. Venkataraman, M. S. Dresselhaus, and G. Dresselhaus, Chem. Phys. Lett. **209**, 77 (1993).
[40] N. Chandra, S. Namilae, and C. Shet, Phys. Rev. B **69**, 94101 (2004).
[41] G. V. Lier, C. V. Alsenoy, V. V. Doren, and P. Geerlings, Chem. Phys. Lett. **325**, 181 (2000).
[42] D. Qian, W. K. Liu, and R. S. Ruoff, J. Phys. Chem. B **105**, 181 (2000).
[43] L. Shen and J. Li, Phys. Rev. B **69**, 45414 (2004).
[44] B. I. Yakobson, C. J. Brabec, and J. Bernholc, Phys. Rev. Lett. **76**, 2511 (1996).
[45] T. Halicioglu, Thin Solid Films **7312**, 11 (1998).
[46] Y. Xia, M. Zhao, Y. Ma, M. Ying, X. Liu, P. Liu, and L. Mei, Phys. Rev. B **65**, 155415 (2002).
[47] E. Hernandez, C. Goze, P. Bernier, and A. Rubio, Appl. Phys. A: Mater. Sci. Process. **68**, 287 (1999).
[48] W. L. Wang, K. J. Liao, C. Z. Cai, C. G. Hu, Y. Ma, and J. W. Lu, *Science and Technology of Nanomaterials* (Trans Tech), (2002), Vol. 23, p. 309.
[49] G. Zhou, W. Duan, and B. Gu, Chem. Phys. Lett. **333**, 344 (2001).
[50] J. P. Lu, Phys. Rev. Lett. **79**, 1297 (1997).
[51] Zhan-chun Tu and Zhong-can Ou-Yang, Phys. Rev. B **65**, 233407 (2002).
[52] D. E. Soule, Phys. Rev. **112**, 698 (1958).